Chemical Engineering Journal 510 (2025) 161128

Contents lists available at ScienceDirect

Chemical Engineering Journal

journal homepage: www.elsevier.com/locate/cej

An innovative data-driven approach to the design and optimization of battery recycling processes

Nima Emami [a], Luis Arturo Gomez-Moreno [b], Anna Klemettinen [b], Rodrigo Serna-Guerrero [b,*], Milica Todorović [a,*]

[a] Department of Mechanical and Materials Engineering, University of Turku, Turku, Finland
[b] Department of Chemical and Metallurgical Engineering, Aalto University, Espoo, Finland

ARTICLE INFO

Keywords:
Data-driven
LIB recycling
Optimization
Simulation
Recovery

ABSTRACT

With the growing demand for raw materials to enable the ongoing electrification transition, robust battery recycling technologies will also become necessary to reduce reliance on primary resources and improve sustainability. To boost the recovery of secondary materials, we combined HSC-Sim® recycling process simulations with data science to analyze the flow of Li-ion battery components through the processing stages. Key operating parameters of the process were varied to assess their impact on material recovery and grade of graphite anode (Gr) and nickel-manganese-cobalt cathode (NMC). The resulting data distributions allowed us to establish if the process design was capable of producing desired recovery outcomes, and under which set of conditions optimal performance could be obtained. Materials flow analysis was utilized to guide decision-making and iteratively redesign the recycling process towards better outcomes. In the final stage, multi-objective optimization was deployed to achieve a balance between maximal NMC mass recovery of 66.3% at 95.7% grade and Gr mass recovery of 88.7% with 99.8% grade. This scalable, data-driven framework could replace intuition-led recycling process trials with rational process design to optimize complex device recycling, accelerating the transition towards more sustainable and effective material recycling.

1. Introduction

The proliferation of Li-ion batteries (LIBs) in today's society is at an all-time high, with applications ranging from electronic portable devices to transportation and large-scale energy storage. The demand for LIBs has exerted immense pressure on the extraction of raw materials needed for their production [18]. LIBs contain a multitude of materials, including graphite (Gr), Al, Cu, Co, Li, Mn, and Ni. Unfortunately, the extraction of these materials is both complex and resource-intensive [8,16,19].

In response to the challenges posed by the currently dominant linear value chain of LIBs, the concept of a circular economy (CE) emerges as a potential solution. CE aims to optimize recycling procedures and minimize resource loss by promoting the continuous recycling of existing materials and products [36]. As part of this effort, the European Union introduced the Circular Economy Action Plan (CEAP) [7], which sets regulatory goals for sustainable battery recycling and material recovery. The CEAP highlights the importance of efficient recycling solutions to recover critical materials and reduce dependency on primary resources.

Beyond the CEAP's regulatory framework, multiple 'R' strategies, such as reduce, reuse, recycle, recover, remanufacture, and repurpose, play a crucial role in circular LIB recycling. Zorpas [49] remarks that these approaches go beyond material recovery by extending the functional life of components, reducing waste, and minimizing environmental impact. Incorporating multiple 'R' strategies into LIB recycling can shift the focus from metallurgical recovery to a more comprehensive resource efficiency approach.

To make this vision a reality, modern, efficient, and sustainable LIB recycling processes are crucial. Industrial-scale LIB recycling processes are already established across various continents, with combined capacities of up to nine hundred thousand metric tons per year [13], although primarily focusing on the recovery of Co, Ni, Mn, Cu, Al and steel. LIB recycling typically follows a metallurgical route, often preceded by mechanical processes [46,47]. These recycling routes are efficient in recovering transition metals in the form of alloys and Li in the slag phase, although at the expense of losing Gr, plastics, and

* Corresponding authors.
E-mail addresses: rodrigo.serna@aalto.fi (R. Serna-Guerrero), milica.todorovic@utu.fi (M. Todorović).

https://doi.org/10.1016/j.cej.2025.161128
Received 20 December 2024; Received in revised form 19 February 2025; Accepted 27 February 2025
Available online 14 March 2025

electrolytes [17]. The mechanical processes, commonly used as pretreatment, also play a crucial role in metallurgical routes, ensuring that battery materials are liberated for efficient recovery, taking advantage of physical properties (e.g., particle size, density, magnetic susceptibility) to facilitate separation [46]. Recently, physical separation operations have gained attention as alternative recycling routes, commonly referred to as direct recycling. The use of direct recycling is appealing since it focuses on recovering materials while maintaining their original structure and composition, in contrast with pyrometallurgical or hydrometallurgical processes that transform them into pure elements or new compounds. Examples of direct recycling include physical separation, electrochemical recovery [10], froth flotation [28] and cathode regeneration [48]. These methods offer a less resource-intensive alternative to the dominant pyrometallurgical and hydrometallurgical processes.

Although these different routes aim to recover valuable materials, due to the characteristics of end-of-life LIBs, these processes can be highly complex. Indeed, the composition of LIBs is intricate, with multiple material species, including metals, plastics, inorganic, and organic compounds. Furthermore, these structures are strongly bonded with adhesive binders, making the separation difficult. The chemical stability of Li salts and electrolytes also complicates their safe recovery [21]. Additionally, the constant development of new cathode chemistries, anode materials and designs intensifies the complexity of recycling and recovery processes for LIBs. Battery waste (known as black mass or BM) nowadays represents a high-entropy blend, whose recycling requires numerous unit operations and a large number of their operating parameters that should be optimized to achieve high-purity products in an economically viable fashion.

In this context, process simulation has become an essential tool for evaluating variations in LIB recycling processes and optimizing operating conditions in a cost-effective manner. By simulating complex systems through mathematical modeling, researchers can assess process variations, identify inefficiencies, and predict potential outcomes. The application of process simulation software in LIB recycling is well-documented, particularly in evaluating process efficiency, environmental impact, and resource recovery strategies.

Several studies have explored simulation-based assessments of LIB recycling. Rinne et al. [25] and Arellano-Sanchez et al. [4] integrated flowsheet simulation and life cycle assessment (LCA) to evaluate emerging hydrometallurgical recycling, focusing on chemical consumption efficiency. Punt et al. [24] developed dynamic flowsheet models for mechanical recycling, examining the role of cutting mills and zig-zag sifters in pretreatment. Ali et al. [2] employed process simulation-based LCA to compare the environmental footprint of secondary and primary materials, emphasizing the importance of process-level data in LCA modeling. Vierunketo et al. [38] introduced exentropy analysis to assess material and energy circularity across different recycling routes, while Tas et al. [32] applied Statistical Entropy Analysis combined with LCA (SELCA) to evaluate sustainability trade-offs in LIB recycling. Baum et al. [5] further highlighted that common LIB recycling processes, particularly pyrometallurgical and hydrometallurgical routes, often prioritize metal recovery over process efficiency, leading to suboptimal material use, an aspect that simulation-based approaches could help address.

While these studies have advanced LIB recycling research, they primarily focus on case-specific evaluations rather than the use of simulation to develop systematic evaluation methodologies. Most simulation-based research assesses parameter sensitivity within fixed scenarios but does not incorporate optimization techniques to explore trade-offs between performance parameters (e.g., grade and recovery). Furthermore, many studies evaluate process performance in isolated steps rather than considering the interactions between unit operations, which significantly impact overall system performance. This limitation is not exclusive to LIB recycling but extends to chemical and process engineering more broadly. As noted by Pistikopoulos & Tian [23], the lack of integrated computational tools constrains systematic assessments of process simulation. The absence of a widely adopted, general-purpose optimization tool for flowsheet simulation further complicates process modeling and comparisons, limiting the ability to refine process conditions.

At the same time, a major challenge in process optimization is the computational burden associated with large-scale simulations. As described by Sinnott [31], optimization methods such as linear programming, dynamic programming, and search algorithms often involve highly nonlinear and discontinuous functions, making optimization computationally expensive. In LIB recycling, the use of unit operations such as flotation, magnetic separation, and leaching are adopted from the mineral processing and metallurgical practice [17,45,46]. Although optimization is evidently needed in these fields, they follow a conventional approach in which only the recovery or grade of a specific component is designated as the optimization target. This is not an ideal scenario for complex materials and products, which reduces confidence in traditional optimization methods and highlights the need for more robust, data-driven approaches that can systematically refine operating conditions.

To address the limitations exposed above, a novel approach hereby explored is the integration of data science with traditional process engineering. The vast amounts of data generated from modern experiments, plant operations, and simulations often surpass the capacity of manual analysis and conventional tools, making it difficult to extract meaningful insights and optimize processes effectively [6]. Data science techniques such as data management, multi-objective optimization, and advanced visualization provide methods to effectively handle and analyze these large datasets, enabling the development of more accurate and efficient evaluation methods for complex systems. Additionally, combining data science and high throughput data generation with simulations enhances these models by facilitating the integration of real-world data [44]. In process engineering, metallurgy, and materials science, data science has become essential for optimizing processes, predicting material properties, and innovating new materials, marking a shift toward the “fourth paradigm of science.” This data-driven approach leverages extensive datasets generated through computational and experimental methods, allowing researchers to understand structure–property relationships that traditional methods might miss [1,15]. High-throughput data generation enables efficient insights into how variations in feed composition or processing conditions influence material properties, streamlining tasks such as alloy design, heat treatment, and phase transformation [39]. By minimizing the need for trial-and-error experimentation, data-driven methods allow rapid exploration of compositional spaces and process parameters, significantly reducing time and resource costs [1].

In this study, the focus is on improving material purity and recovery from the direct recycling of cathode and anode materials using froth flotation, following the experimental work previously published by Vanderbuggen et al. [35], Ruismaki et al. [27], and Saneie et al. [29]. Our objective is to implement a new data-driven approach to evaluate the potential of proposed recycling processes. For each process, high-throughput data analysis is performed to assess numerous possible outcomes as a function of key process parameters, helping to determine each process’s advantages and limitations. This information is subsequently used to refine and improve the simulated process. To achieve this, comprehensive literature data was collected to design a recycling process simulation based on commonly used unit operations. The process simulation was implemented in HSC-Sim® process simulation software, where critical operating parameters were varied within realistic value ranges. In parallel, we conducted a high-throughput exploration of process outcomes as a function of these parameters through Python API workflows on a supercomputer. This approach allowed for analyzing large datasets to identify patterns, correlations, and potential process limitations, which would not be apparent from a limited set of simulations. Key success metrics include improved mass recovery and

purity (grade) of two critical materials: NMC and Gr. By the end of the study, we demonstrate how process outcomes can be optimized based on our analysis. Our iterative methodology enables the identification and optimization of new process configurations by analyzing large datasets to address inefficiencies and key issues, potentially revealing non-obvious solutions. This manuscript presents a novel, generalizable approach to recycling process design and optimization using high-throughput data analytics facilitated by supercomputing workflows, which could be broadly deployed in sustainable metallurgy applications targeting different parameters, materials, and metrics. Our method leverages extensive data and thousands of simulations upfront to determine early on whether specific targets are feasible, reducing reliance on trial-and-error optimization in process design.

2. Materials and methods

This study introduces a new computational framework to simulate and analyze a recycling process. Such an approach requires a framework for simulating a recycling process, along with the definition of the input feed materials and the relevant process parameters. Next, specialized parallelized computation is needed to carry out the high-throughput simulations and screen 10,000 process variations and outcomes. Specific metrics for process success are necessary to evaluate process capabilities so that the process can be modified and optimized. For each process, data analytics can be carried out to establish which process variables and settings optimize the outcomes. To ensure a clear understanding of our methodology, the following subsections will detail each step, starting from the simulation method and process description, followed by high-throughput process variations and optimization strategies.

2.1. Simulation method and process description

In the subsequent section, we describe the simulation tools and design considerations that underpin our recycling process model. The simulation processes were conducted using HSC-Sim® version 10.2.2 [3]. For this study, the mineral processing unit was used to illustrate a simple pre-treatment and direct recycling process for end-of-life LIBs. Mineral processing model units encompass a wide range of unit operations, including crushing, milling, screening, and magnetic separation, among others. In the HSC-Sim® simulation, we used a particle-based model, incorporating size and chemical composition.

2.2. Black mass input feed

To simulate any process, the material input feed representing a typical BM must first be established. Here, the feed material consists of $Li(Ni_1Mn_1Co_1)O_2$ (NMC) type end-of-life batteries. It is assumed that the batteries have previously undergone a crushing process and a thermal treatment, which disassembled battery cells and removed any liquid compounds, such as the organic electrolyte solvent typically found in LIBs. This is a relevant simplification since modeling a liquid other than water in HSC-Sim® adds unnecessary complexity to the system. For HSC-Sim® mineral processing units, two properties are required to describe input feed: mineral species composition and distribution by size [3]. In the present work, the feed comprises eight different materials: casing, anode, cathode, current collectors for both anodes, electrolyte (assumed to be composed of only a solid salt), and plastic separator. A literature review was performed to establish a typical input feed for NMC-type BM (See Supplementary Data SD Section S1). The input mass flow was set at 100 t h^{-1}, with the bulk and cumulative size compositions detailed in Fig. 1. Having established the input feed parameters, we next outline the specific recycling process units employed in our study.

2.3. Recycling process simulation

The simulated recycling process is composed as a sequence of HSC-Sim® unit operation models, each representing a typical processing step. The initial hypothetical process design (P1) relies on experimental data from the literature, supported by various assumptions made at different stages of the process. These include, for example, the evaporation of the solvent in the electrolyte, the pre-crushing of battery cells, and the selection of a specific model behind a unit operation, among others. Detailed information on the simulation setup, including all assumptions, parameters, and the models used for the unit operations, is provided in the SD sections S1 and S2.

Admittedly, the reliability of the process simulation depends on the accuracy of the models used in each unit operation, as their applicability is constrained by material properties, operating conditions, and available experimental data. Therefore, understanding the process flow and its individual steps is critical to assessing both the validity of the models and the simulation outcomes.

As shown in Fig. 2, the process starts with particle size reduction, followed by magnetic separation to produce magnetic and non-magnetic streams. The non-magnetic materials undergo screening for a second particle size reduction. Two fractions are created: the overflow stream is passed on to milling while the underflow stream enters directly into the

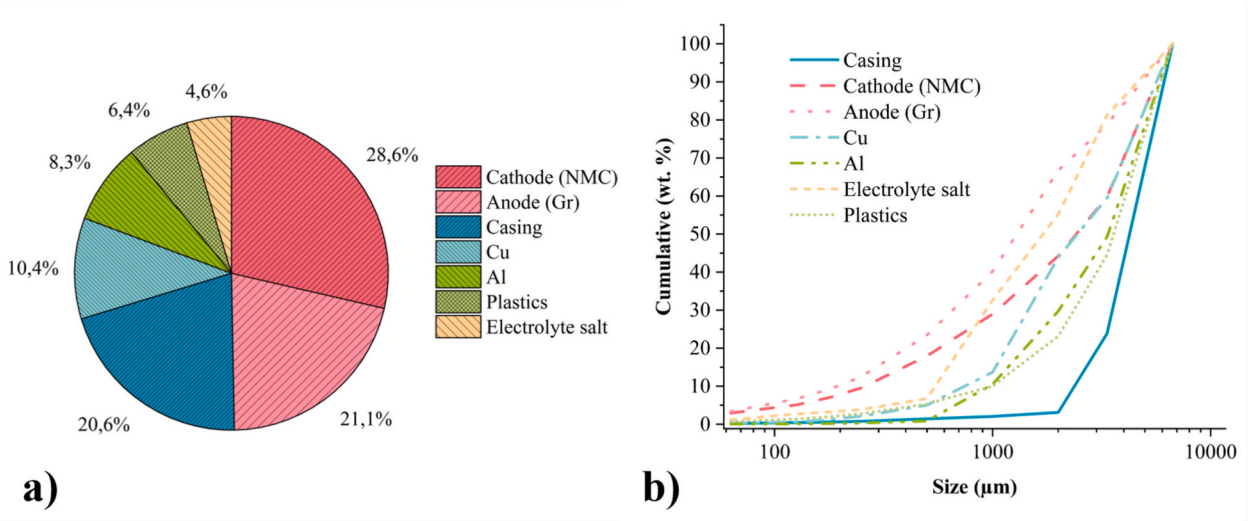

Fig. 1. a) Feed composition in wt. % and b) cumulative composition by size.

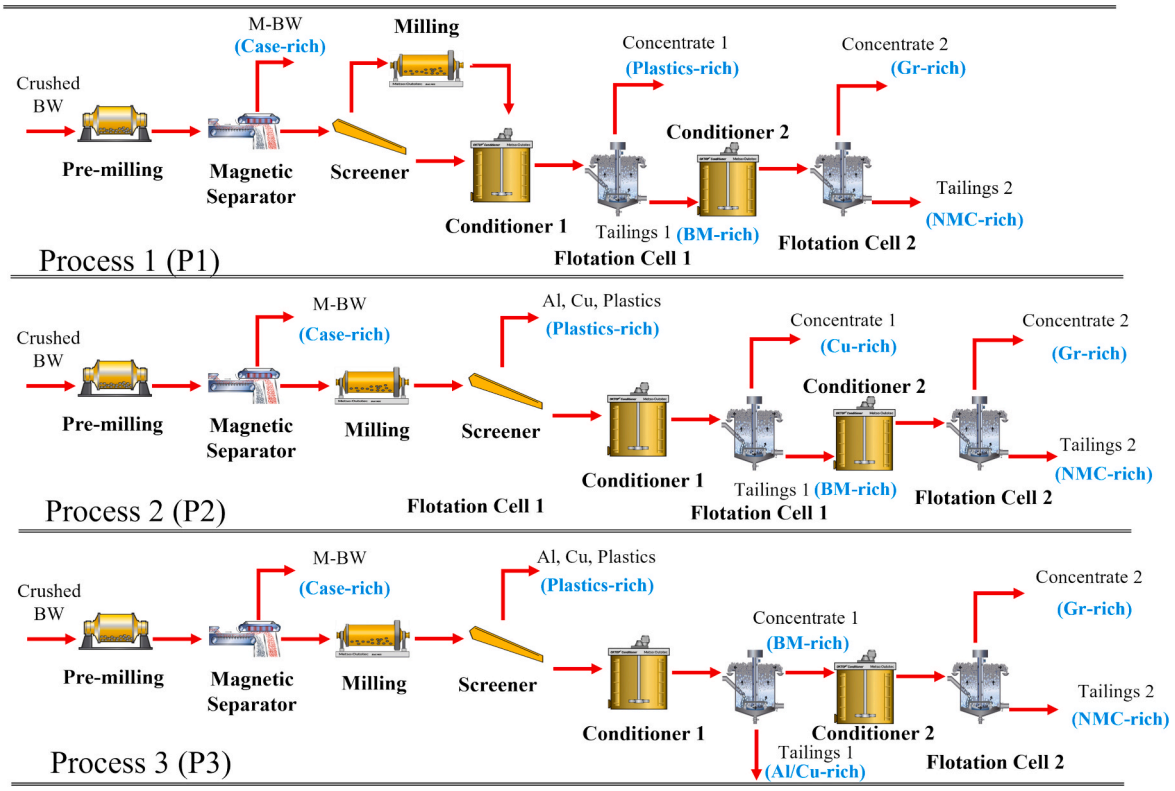

Fig. 2. (P1) Initial process hypothesis for a sequence of unit operations to describe mineral processing LIB recycling, second iteration (P2) and (P3) refined process hypothesis.

next stage. The undersized and milled fractions simultaneously enter a froth flotation circuit consisting of two sequential flotation units, each with its own conditioner, to produce two distinct material concentrates, resulting in a total of three output streams. In the subsequent iterations of the recycling process design (P2 and P3 of Fig. 2), most of the same unit operations were retained, with slight differences in the materials recovered and the function of certain units. With the simulation method in place, we proceeded to explore high-throughput variations to ensure comprehensive coverage of process parameters.

2.4. High-throughput process variation

Each unit operation in HSC-Sim® offers a wide range of modifiable parameters. These include simulation settings, such as tolerance for mass balance convergence, and process-specific parameters, such as the product size P_{80} in a milling operation. In the context of this research, these parameters were divided into three categories. The simulation parameters that either do not contribute much to the final outcome of the model, or are not feasible to change, were fixed to default values (Tables S4 and S5). Other process model parameters (i.e. calibration parameters) were set to specific values to suit our process design, but we did change some of them between process iterations (see Table S6). Parameters that could directly affect the outcomes and are critical to the final recovery of materials are indicated in Table 1. The table presents the defined upper and lower bounds for each parameter, outlining the ranges within which these parameters were varied during high-throughput process exploration. For some parameters, these bounds were adjusted across different process iterations based on the observed outcomes, reflecting the dynamic nature of the process design and the optimization efforts undertaken.

The next step after defining the process stages was the high-throughput data generation by random selection of 10,000 combinations of variable operating parameters. The random selection enabled us to capture a wide range of possible outcomes and scenarios within the modeled process. Subsequent HSC-Sim® simulations resulted in a comprehensive dataset of thousands of possible process outcomes that provides unbiased coverage across the search space.

Here, HSC-Sim® mineral processing units generated a wide range of process data for each unit, including mass flow, volumetric flow, slurry flow, specific gravity (SG), solids content, particle size (P_{80} and P_{50}), elemental and component composition (grade), and mass recovery (the fraction of material recovered at a specific stream relative to the feed). For this study, the focus was on the mass recovery (M_n %) and grade (wt. %) of NMC and Gr from the final output streams were selected. These metrics were chosen to evaluate recycling process performance in terms of materials separation (grade) and recovery.

Table 1
Variable parameters used in the simulation with their range for the P1, P2 and P3.

Process	Parameter (Unit)	P1	P2	P3
Pre-milling	Specific Grinding Energy (kWh t^{-1})	0.01 – 6	–	–
	Rosin-Rammler Slope (–)	0.1 – 3	–	–
Magnetic Separator	Magnetic Field Strength (Tesla)	0.01 – 5	0.01 – 0.5	–
	Interstitial Velocity (m s^{-1})	0.01 – 3	–	–
	Saturation Magnetic Field Strength (Tesla)	0.01 – 5	x	x
Screener	Nominal Aperture Size (mm)	0.1 – 3	–	–
	Separation Sharpness α (–)	1 – 15	–	–
Milling	Specific Grinding Energy (kWh t^{-1})	0.01 – 6	–	–
	Rosin-Rammler Slope (–)	0.1 – 3	–	–
Flotation Cell 1	Fixed Residence Time Target (min)	0.01 – 30	–	0.01 – 40
Flotation Cell 2	Fixed Residence Time Target (min)	0.01 – 30	–	0.01 – 40

Using the defined metrics, multiple histograms were generated for the M_n and grade of both NMC and Gr. These histograms reveal the distributions of process outcomes across all 10,000 simulations. Analyzing these data helped us better understand the process limitations and identify any process tendencies (biases), limitations and outliers. This information was analyzed and used to modify the process toward better performance.

2.5. Computation implementation

After defining the simulation process and generating high-throughput data, we implemented a computational framework to manage and execute these simulations efficiently, as described in the following section. The HSC-Sim® software is typically utilized through a Graphical User Interface (GUI) on Windows OS, which supports process analysis but presents challenges for big data process exploration. High-throughput process analysis is hindered by the GUI-based sequential user workflows and parallel computing is made difficult by the Windows platform. In this study, the less-known Application Programming Interface (API) of HSC-Sim® was exploited to switch away from the GUI and use scripts instead. This methodology was previously introduced in detail by Emami et al. [11], which can be consulted for further details. The API in Windows.NET programming language was integrated with Python3 scripts to develop a parallelized computing workflow. All computational work was performed in the Windows OS environment using the cPouta cloud computing service running Intel Xeon Cascade-lake processors at the CSC-IT Center for Science, Finland's national supercomputing facility.

While independent (so-called "embarrassingly parallel") simulations were facilitated by a randomized sampling of process variables, several data generation algorithms were tested for best parallel efficiency and fastest computation. Here, we combined both the HSC-Sim® native parallelization strategies with Python API parallelization. The optimal algorithm is illustrated in Fig. S6. Given a list of 10,000 randomly selected process variables and N CPU cores, HSC-Sim® API was engaged multiple times to initiate N parallel workflows. Each workflow was managed by HSC-Sim's® own parallelization routines, allowing each CPU to receive a sequence of dynamically allocated process instances to compute until the total list of process variations was exhausted across all N CPUs.

This workflow was benchmarked with an increasing number of CPUs to establish the best working efficiency in Table S7. While computational time was reduced with increasing computer resources (as expected), the parallel efficiency was sub-optimal, and after 8 CPUs, the total computing time began to rise. Timing analysis of individual algorithm stages revealed that establishing the HSC-Sim® API connection was by far the most computationally costly operation. While more CPUs favor the embarrassingly parallel computations, they also increased the number of API connections and, thus, the total simulation time. Optimal timing results were observed with 8 CPUs, with 10,000 points computed in 3.4 h, and all computational work was performed in this way. From each process simulation, it was possible to extract material flow information stored in HSC-Sim® variables for any material and stream. This allows to compute the relevant process metrics for materials recovery and purity. The method development work presented above can now be generally deployed to parallelize any HSC-Sim® simulations and facilitate big-data generation in sustainable process engineering.

2.6. Multiobjective optimization (MOO)

The optimal outcome in a recycling process is one where every material is efficiently separated with both high M_n and purity. In this work, we sought to maximize four objectives: mass recovery and grade of NMC and Gr in the output streams of the final process unit. While 10,000 process variations were analyzed to establish conditions that optimize these outcomes, it is highly likely that different processing conditions achieve each one of the objectives. For example, process operational parameters that maximize Gr recovery may not lead to good purity of recovered Gr nor maximize NMC recovery. A multiobjective optimization (MOO) approach is required to optimize materials recovery with conflicting objectives.

Based on all available process variations, the MOO algorithm identifies a subset of solutions that represent optimal trade-offs between various outcomes. This subset comprises the Pareto front [33]. Pareto points indicate the best possible compromise between objectives; no solution on the front can improve one objective without worsening another. Basically, this algorithm filters out less favorable solutions, leaving only those that offer the best balance between the objectives. By studying the range of Pareto optimal solutions, it is possible to explore different compromises suggested by the data, and identify ones that are most useful in process engineering.

After the Pareto-optimal solutions were identified in 4-dimensional space of objectives, we set out to select the processing conditions that produced the overall best performance. This task was addressed by a MOO procedure based on distance from a hypothetical best outcome [9]. Among all the Pareto solutions, the best outcomes for each of the four objectives were identified, regardless of the fact that different processes were needed to achieve them. They were combined into a theoretical (and unachievable) best solution in 4-dimensional space. For each process variation on the Pareto front, the Euclidian vector distance (L2 norm) from this ideal solution was evaluated. After ranking the Pareto points by distance from the ideal, the solutions closest to the optimum were selected and further analyzed. This approach additionally allows to weigh the different objectives by relative importance. In this way, expert knowledge about recycling needs can be incorporated into the models to identify the overall optimal solutions that are also the most useful in practice. This methodology provides insights not only into the best process settings but also into potential trade-offs that may need to be accepted in practical implementations.

3. Results and discussion

Below, we present the distribution of simulated process outcomes as a function of operational parameters, with a focus on mass recovery and purity of Gr and NMC. Data on the materials flow, and especially the best and worst possible outcomes, were analyzed and utilized to iterate process design. After process modifications, the high-throughput study was repeated and the capabilities of the new process were evaluated. In this way, we demonstrate how process engineering expertise can be combined with data analytics to iteratively improve materials separation outcomes. In the last step, we identified the process parameters that simultaneously optimize materials recovery and purity.

3.1. Analysis of P1 performance and consequent process modification

The statistical distributions of the 10,000 outcomes of the process variations for P1 are shown in Fig. 3a). The distributions illustrate the mass flow and grade of products at the final flotation process stage, namely Gr in the float stream and NMC in the sink stream. These distributions help visualize the spread of potential outcomes of the selected process P1, reflecting its capability to reach separation targets. The simulation data for grade and mass flow for all materials in all the streams was additionally analyzed for a comprehensive understanding of the process behavior (not shown due to space limitations).

The P1 results for NMC indicate there is potential for mass recovery and grade that improve on the input feed. Both mass recovery and grade exhibit a broad distribution with a strong bias towards suboptimal low outcomes, but many process variations also produced higher outcomes. Concretely, NMC mass recovery could be as high as 60.6 %, although the average of 3.2 % indicates much scope for improvement. The findings for NMC grade follow a similar pattern. The average grade is 7 %, but some process parameters achieve NMC purity of 56.5 %, which

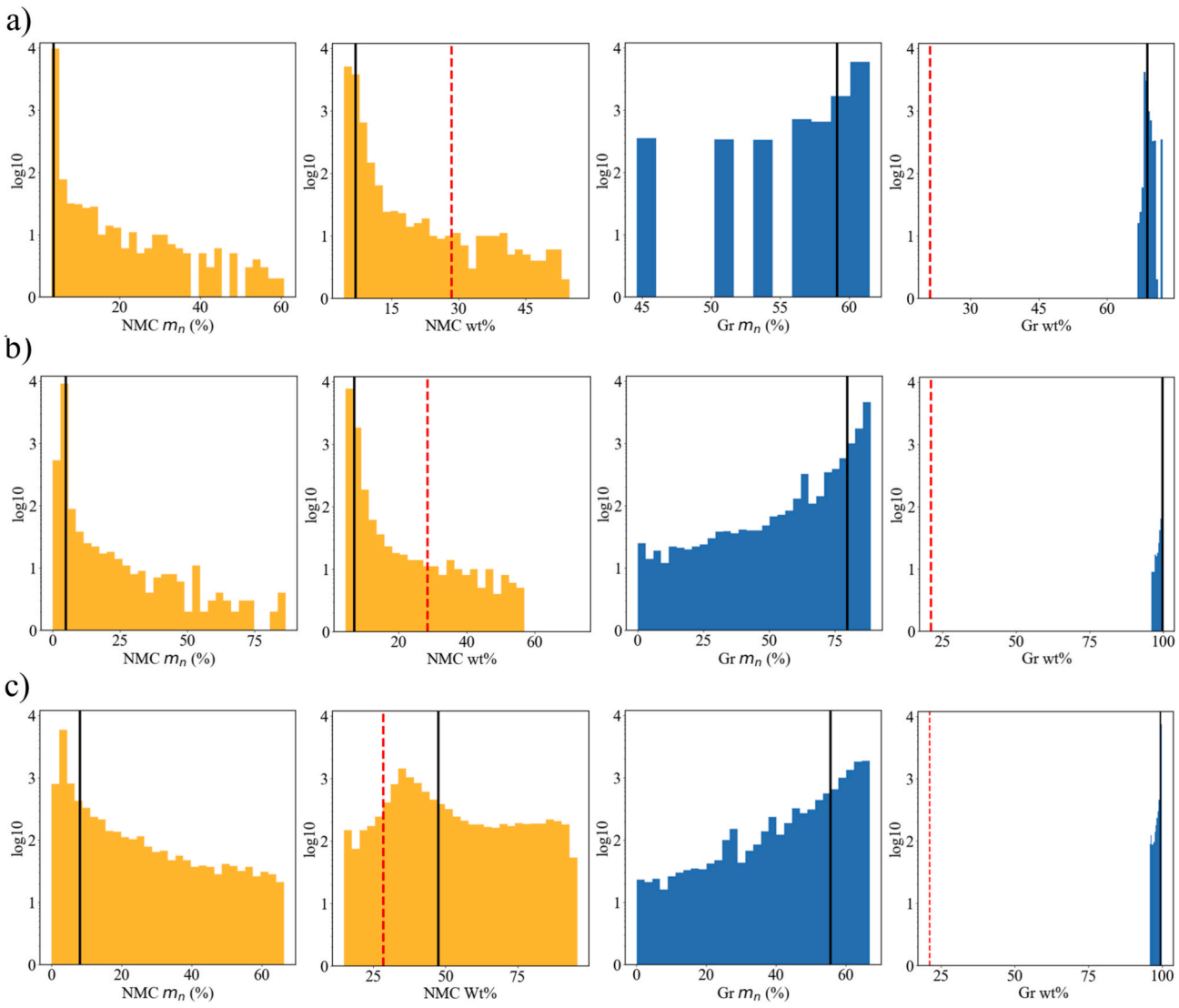

Fig. 3. Distributions of mass and grade for NMC and Gr in the tailings and concentrate streams across 10,000 simulations for three processes. The black line represents the mean value, and the red dashed line indicates the input mass or weight percent. (a) P1, (b) P2, and (c) P3. Each subplot includes NMC grade in the tailings, NMC normalized mass in the tailings, Gr grade in the concentrate, and Gr mass flow in the concentrate.

surpasses original NMC grade in the input feed. P1 process outcomes for Gr differ qualitatively from NMC ones. Gr recovery distribution is not as broad as the NMC one, and is biased towards higher values with a mean at 59 %. The highest recovery observed was 61.8 %. In contrast, Gr grade distribution was very narrow, reaching the best result of 68.9 %. This indicates that Gr enrichment occurred under all combinations of operating conditions in process P1. Overall, we observed reasonable separation outcomes for Gr, but P1 did not separate NMC well (See Table 2).

To understand the fundamental causes of these results, a comprehensive material flow analysis was conducted, revealing two key process limitations: the magnetic separator and the screener processing units. The P1 magnetic separator was intended to separate only the casing, leaving the remaining materials for Flotation Cell 1. However, the separator was capturing substantial amounts of NMC along with the casing. The P1 magnetic separator was simulated as a high-intensity unit, typically used to concentrate weakly magnetic minerals like hematite, chromite, and wolframite [40]. NMC is weakly attracted to magnetic fields, being a paramagnetic material due to its magnetic susceptibility [14]. Therefore, it was theoretically possible to separate NMC particles, as their magnetic susceptibility is close to that of $LiFePO_4$ (LFP), another cathode material that has been successfully separated from black mass using this type of magnetic separator [14]. With the magnetic field varied from 0.01 to 5 T (refer to Table 1), in about 60 % of process variations the magnetic field exceeded 3.6 T, the theoretical value required to capture NMC particles. In many instances, NMC was

Table 2
Target material (stream) property outcomes and distribution statistics for different processes simulated.

Process	Material	Property	Range (%)	Mean (%)	Input Feed (%)
P1	NMC (Tailing)	M_n	3.2–60.7	1.6	–
		wt.%	4.4–56.5	7.0	28.5
P1	Gr	M_n	44.6–61.5	18.3	–
	(Concentrate)	wt.%	66.7–72.2	68.9	21.1
P2	NMC (Tailing)	M_n	0.0–86.5	2.1	–
		wt.%	4.5–72.9	7.0	28.5
P2	Gr	M_n	0.1–88.7	24.1	–
	(Concentrate)	wt.%	95.3–99.9	99.8	21.1
P3	NMC (Tailing)	M_n	0.0–66.3	3.5	–
		wt.%	14.8–95.2	47.3	28.5
P3	Gr	M_n	0.1–66.9	17.2	–
	(Concentrate)	wt.%	95.8–99.8	99.4	21.1

extracted from P1 at this stage, leading to a broad distribution of NMC recovery and grade in Fig. 4a) and overall poor mass recovery in the final stage. Gr was not separated at all by the magnetic separator since it is a diamagnetic material with a negative magnetic susceptibility [12]. The relatively inefficient magnetic separation caused Al, Cu and other materials to reach the screener, which presented the second problem. The screener was designed to produce two distinct streams: one over 500 μm, intended for milling before entering the first flotation cell, and another below 500 μm, meant to be fed directly into flotation. The main objective of the screener was thus to prepare the black mass for froth flotation, as studies [29] have shown that froth flotation can effectively recover plastics. Given inefficient magnetic separation and no output streams at the screener stage, Al, Cu, and S. electrolyte passed through the first flotation stage (where they could not be separated) and reduced the selectivity for NMC and Gr in the final stage.

Addressing these inefficiencies required modifications to the process design, which informed the refinement towards P2. The range of magnetic field strength in the magnetic separator was changed to include the possibility of operating also a low-intensity magnetic separator. The screener stage, which previously sent particles below 500 μm directly to the first froth flotation stage, was repurposed. The milling operation now served as a pre-treatment unit for subsequent froth flotation units, while the screener was adapted to separate large particles of materials that are harder to break, such as plastics and Al and Cu foils. Consequently, the first flotation stage was repurposed for Cu separation, following the work by [29]. Although Cu foils are not naturally hydrophobic, the aforementioned study showed that it can be hydrophobized by surface activation with sodium sulfide (Na_2S) and then separated using potassium amyl xanthate (PAX) as a collector. The flowsheet for the resulting design is shown in Fig. 2 P2) and detailed changes for all parameters can be found in the SD.

3.2. Analysis of P2 performance and consequent process modification

Following the high-throughput P2 simulations, the distributions of mass recovery and grade for NMC and Gr products are illustrated in Fig. 3b). Again, NMC data exhibits a broad distribution heavily biased towards low values, with a tail reaching the best possible values. The average P2 NMC outcomes were very similar to those observed in P1, but the optimal outcomes were notably better. NMC M_n reached a maximum of 86.5 %, and the grade could be as high as 2.9 %. Considerable improvements over P1 results were also observed for Gr. Purity was now consistently high, with a very narrow distribution centered around 99.8 %. The Gr mass recovery distribution was very broader than before, but still biased towards high mass values. P2 was capable of recovering up to 88.7 % of Gr from the input feed. It is clear that P2 improved on the separation targets for both NMC and Gr, with the latter approaching optimal outcomes. A comprehensive material flow analysis was carried out to understand the mechanisms behind this change.

This analysis informed two critical modifications in P2: an expanded calibration of the magnetic separator and the addition of a new output stream to improve selectivity. These improvements enhanced the recovery of NMC and Gr by allowing both high and low intensity in the magnetic separator and adding a new separator output stream. Typically, low-intensity magnetic separators are used to separate ferromagnetic materials from para and diamagnetic materials. In mineral processing, such examples include the recovery of magnetite (F_3O_4), hematite (Fe_2O_3), and siderite ($FeCO_3$) [40]. In recycling, low-intensity separators are commonly applied in processes such as scrap steel recovery, automobile recycling, construction waste, electronic waste, plastic, and glass separation [41]. For LIB recycling, the use of low-intensity magnetic separation is well-documented in several studies [36,43,46,47], for recovering ferromagnetic materials like casing. However, specific types and intensities of magnetic separators are rarely reported, so we were unable to use appropriate settings from the outset. In P2, NMC was less affected by the magnetic separator due to the lower magnetic field gradient (1 T/mm). Mass flow analysis helped us establish that low magnetic field strength of 0.5 allows NMC flow to the final process stages.

Paradoxically, the introduction of an additional output stream in the screener, meant to recover other materials and prevent them from reaching the last flotation cell, also reduced the recovery of NMC by removing it from the process. Both NMC and Gr are electrode active materials, coated onto Al and Cu foils, respectively. The cathode foil has an adhesive strength of 1.0 N/mm^2 [42], making it difficult to liberate from the Al foil. Wuschke and collaborators (2019) [42] reported that only around 6 to 25 % of cathode particles are smaller than 10,000 μm when subjected to pre-crushed battery cells to grinding [42]. Efficient cathode liberation is possible with appropriate mechanical de-lamination, which occurs through forces such as shear, cutting, and tearing during crushing, shredding, or milling [30]. Al foil, being ductile, deforms but largely remains intact, while NMC particles are separated into smaller sizes (<100 μm) [34], with some studies even reporting ultrafine particles (< 10 μm) after mechanical treatment [26]. This creates various scenarios in the simulations where low energy (SGE), leading to less intense milling, produces large P_{80} values (> 1000 μm) and screen aperture sizes above 2000 μm, resulting in high NMC recovery due to inefficient de-lamination from Al. Gr was similarly affected, though to a lesser extent, as the adhesive strength of the anode foil is 0.4 N/mm^2, lower than that of the cathode [42]. This is evident in the wider Gr recovery distribution in Flotation Cell 2 of P2 compared to P1, while still achieving higher recoveries than NMC.

While P2 demonstrated a more stable and predictable process, particularly for Gr recovery, increased variability in NMC recovery indicated that further optimization was needed. To address this variability and enhance overall recovery efficiency, two major modifications were introduced in P3. The purpose of the first stage of the froth flotation was modified to separate metallic impurities (mostly Cu and Al foils) in the sink stream and produce a rich Gr and cathode stream in the concentrate, better suited for enrichment in the last froth flotation unit. In addition, the operating range of the magnetic separator was modified, selecting only low magnetic intensities (<0.5 T) since it appears that low-intensity magnetic separation favors the retention of NMC in the process.

3.3. Analysis of P3 performance

Fig. 3c) visualizes the distributions of NMC and Gr M_n and grade following high-throughput explorations of P3. For NMC, it was immediately clear that the distribution bias was reduced compared to P1 and P2, with more process parameters producing better outcomes. The best achievable mass recovery was 66.3 %, which is better than P1 but not as good as in P2. However, P3 could achieve NMC purity as high as 95.2 %, a dramatic improvement. The purity of Gr remained excellent, with a narrow distribution averaging around 99.4 %. This time the Gr mass recovery distribution was less broad than in P2, but the best possible mass recovery was reduced to 66.9 %: a result that improves on P1 but is slightly poorer than in P2.

Changes in P1 and P2 to the magnetic separator model served to transform its function from a high-intensity, high-gradient magnetic separator to a low-intensity one. This was achieved by modifying the gradient and calibrating the HSC-Sim® existing model. This resulted in a lower number of simulations producing a high NMC recovery (i.e., >70 %) in the magnetic stream in P3 compared with P1 and P2. While this was a move in the positive direction, it shows that NMC remains suceptible to separation even under fields of low magnetic intensity. In recently published work on LIB chemistries, the Li-Fe phosphate (LFP) cathode had been effectively separated using high-gradient magnetic separators in both simulations and practice, achieving a recovery of 54 % at intensities as low as 0.4 T [46]. NMC has a magnetic susceptibility twice as high than that of LFP (both being paramagnetic), and could theoretically be recovered at 0.5 T in the magnetic stream. This is

perhaps reflected in the magnetic separation behavior predicted by HSC-Sim®. Nevertheless, the wider distribution of NMC in P3 compared to the previous process designs indicates an increase in the number of scenarios where higher NMC grades are achievable in the final product.

The second modification in P3 was the repurposing of the first flotation stage to recover both Cu and Al in the tailings. Ruismaki's work [27] demonstrated that metals such as Al and Cu could be recovered from spent black mass via froth flotation, using kerosene as a collector and MIBC as a frother. In P3, this stage was adapted to separate these materials, leaving only the cathode active material (which still contains binders that make it hydrophobic) and Gr (naturally hydrophobic) to float to the next stage [27,34]. This approach provided key benefits: recovering Al and Cu in a second separate stream, preventing other materials from reaching the second froth flotation stage, and ensuring that only graphite and NMC proceed, which enhanced the recovery of both materials in the second stage, especially NMC. Overall, P3 resulted in high probabilities of acceptable Gr recovery and purity levels. The increase in the mean NMC grade indicates improved recovery, though the high variability suggests further optimization is still possible. These differences highlight the impact of the modifications made in P3, particularly in enhancing NMC recovery, while also maintaining the high performance in Gr recovery.

Based on the large data sets obtained, general trends can be identified in each process scenario, highlighting its possible advantages and bottlenecks. The distribution of performance parameters can also identify suboptimal processes. For instance:

The narrow distribution range of Gr grade produced with P1 reflects a stable process for Gr enrichment. However, the recovery and grade of NMC was inconsistent and below the expected targets, indicating a poor process design.

P2 was able to produce a Gr grade above 90 % and, under specific operating conditions, both NMC recovery and Gr grade approached target levels. However, NMC recovery remains highly variable. This suggests that P2 is a superior design compared with P1, although it is not quite robust. One reason for this is that, while the repurposed screener effectively removes unwanted materials, it also causes some NMC loss, creating a trade-off between selectivity and recovery.

Finally, P3 achieved the highest NMC grade (95.2 %) of all processes through a two-stage flotation. It also demonstrates greater consistency, reducing low-recovery scenarios overall. This is a more consistent design although its productivity remains sensitive to magnetic field settings, which can capture paramagnetic NMC. Balancing flotation and screening parameters remain challenging, sometimes leading to lower recoveries of either NMC or Gr.

3.4. Multi-objective optimization

The P3 process proved to be most reliable in achieving all four objectives of NMC and Gr grade and mass recovery. Based on P3 materials flow data, we proceeded with 4-dimensional MOO and identified 2040 Pareto-optimal points. This means that approximately 21 % of the process variations tested belong to the Pareto front. Fig. 4 illustrates the spatial distribution of the Pareto solutions. Because 4-dimensional spaces are difficult to visualize, we demonstrate a 2-dimensional cross-section in the space of Gr M_n vs. NMC M_n in Fig. 4 a) and another in the space of Gr wt% vs. NMC wt% in Fig. 4 b). In the M_n plot, the optimal solutions are clustered along the right side of the plot because high Gr mass recovery is easier to achieve in this process than NMC recovery. Similarly, the wt% plot illustrates the narrow and high range of Gr grade compared to the much broader range of NMC grade solutions. It is immediately clear that not all solutions are optimal for both NMC and Gr. Next, we proceeded to identify the process variations that lead to the best overall outcomes.

As described in Section 2.4, we identified the optimal objective outcome for each dimension separately. The resulting theoretical optimum is [M_n NMC, M_n Gr, wt% NMC, wt% Gr] = [66.3, 95, 65.3, 99.8] in units of %. Next, we ranked all Pareto points according to the Euclidean distance d_{OPT} from this point, while considering the relative importance of different objectives. Recognizing that high purity is irrelevant without high mass recovery, the weights were adjusted to prioritize mass recovery over grade. Further tests were performed to establish the optimal strategy: the weights for the M_n of both NMC and Gr were set to high priority (numerical value 6), while the weights for material purity were varied between low, medium, and high priority (equivalent to values 1, 3 and 6). The simulations where all objectives had high priority correspond to equal importance among objectives .

The results, summarized in Table 3, indicate that setting the weight for grade to low priority compared to mass leads to the best solution (opt1 in the Table), closest to the theoretical optimum. This allowed to achieve the highest NMC recovery, while still maintaining high recovery and acceptable grade for Gr. In contrast, assigning higher weights to grade significantly reduced NMC recovery, moving away from the optimal balance between objectives. These optimal points are projected onto the 2-dimensional cross-sections of objectives in Fig. 4. The mass cross-section in Fig. 4a) clearly demonstrates why opt1 presents the best compromise between objectives. In the grade cross-section in Fig. 4b), it appears that this solution degrades the wt% of Gr, but the minimum value of 95 % is already so high that the overall solution is still very good quality. Next, we extracted the specific process parameters that produced the opt1 solution and we proceed to analyze them. The optimal process settings are listed in Table 4.

3.5. Insight into optimal process operations

These findings, derived from the data-driven multi-objective optimization strategy, provide valuable insights for designing and optimizing recycling processes in industrial applications. The following is an interpretation of the optimal P3 operational parameters in Table 4.

3.5.1. Pre-milling

The pre-milling unit, with a SGE of 4.49 kWh t^{-1} and a slope of 1.4, reduces the particle size (P_{80}) from approximately 4,900 μm to 165 μm, indicating a significant reduction. Comminution is crucial in the recycling process as it facilitates the liberation of the various battery components. It also prepares the feed material for separators such as froth flotation, where particle size distribution and liberation degree are critical for material recovery [42]. Therefore, it's not surprising that the optimal SGE for the pre-milling unit is high. As demonstrated in other studies [42], proper liberation from steel housing (as in this case) demands a specific energy consumption of 3.5 kWh t^{-1}, which is lower to the 4.49 kWh t^{-1} obtained in this study.

It appears that the model considers a higher production of fines as beneficial. This reflects the generally accepted trend that liberation improves with decreasing particle size. Such trends have been validated in other studies, for example, [22], where various particle size fractions are obtained after attrition milling of shredded LIB packs. Accordingly, the finest fraction (i.e., < 500 μm) contained the highest concentration of both anode and cathode active materials. Modeling the particle size distribution (PSD) also represents a challenging aspect of process simulation. In experimental work, comminution equipment produces PSDs that vary with the composition and size of the materials. For example, Fig. 1 shows that materials like casing, Al, Cu, and plastics tend to have larger particle sizes compared to NMC and Gr. However, in the PSD shown in Fig. 4b, only Cu and Al have a P_{80} above 180 μm, with the remaining materials showing similar PSDs. This reveals the limitations of using a model that relies solely on Bond's equation. Nonetheless, the model provides useful guidance for the type of PSD needed to achieve the highest grade and recovery of NMC and Gr in this case.

3.5.2. Magnetic separator

The magnetic separator represents a special case when using HSC-Sim®, as the default model available is a high-intensity, high-gradient

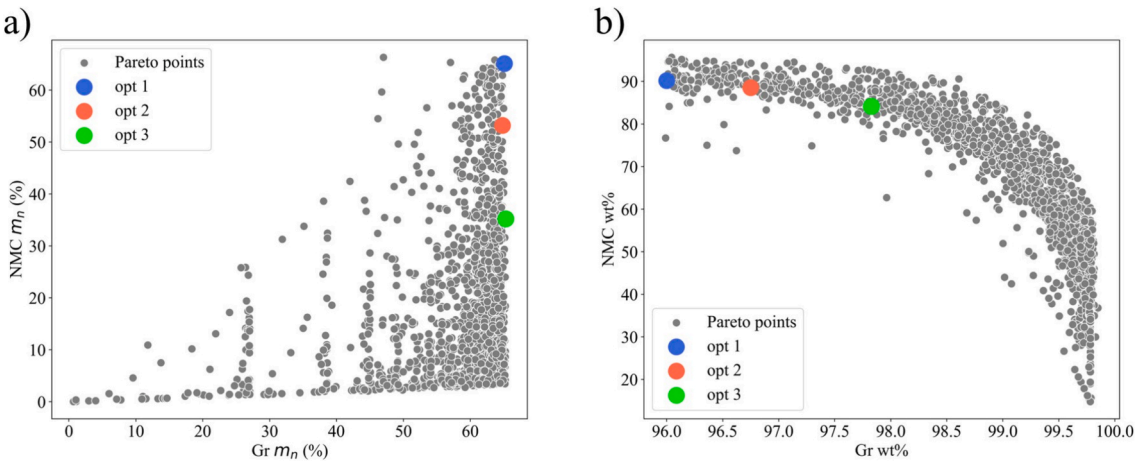

Fig. 4. 2-dimensional cross-section of (a) Gr M_n vs NMC M_n and (b) Gr wt% vs NMC wt% of 4-dimensional space of NMC and Gr M_n and wt%. Pareto-optimal points are indicated in gray, with optimal points from Table 3 shown in colour.

Table 3
Weight combinations used for 4D MOO with M_n always set to maximum. Each solution reflects a different prioritization: (opt1) Strong priority for M_n over wt.%; (opt2) Medium priority for wt.% and high for M_n; (opt3) Equal priority for all variables. The ratio between weights defines the relative importance, with equal scaling (e.g., all weights set to 6 or 1) resulting in the same prioritization. Pareto ranges describe 2040 Pareto points.

ID	NMC wt.% w	NMC M_n w	Gr wt.% w	Gr M_n w	NMC (wt.%)	NMC M_n (%)	Gr (wt.%)	Gr M_n (%)	d_{opt}
opt 1	1	6	1	6	90.9	65.1	96.0	65.1	1.0
opt 2	3	6	3	6	88.5	53.2	96.7	64.8	2.7
opt 3	6	6	6	6	84.1	35.2	97.8	65.3	4.3
Pareto range		–			14.0–95.0	0–66.3	95–99.8	0–65.3	–

Table 4
Optimal parameter values (opt1) for the highest mass recovery and grade of NMC and Gr in P3.

Pre-Milling		**Magnetic Separator**		**Screener**		**Milling**		**Cell 1 and 2**	
SGE (kWh t^{-1})	Slope	Intensity (T)	Velocity (m s^{-1})	Aperture Size (mm)	α	SGE (kWh t^{-1})	Slope	R. time (min)	
4.49	1.4	0.008	2.25	2.5	14	5.61	2.1	36	38

magnetic separator. This type of separator is typically used to separate materials with low magnetic susceptibility, unlike the steel casing intended in the LIB recycling process. The optimal magnetic field intensity for this case is quite low at 0.08 T, with an interstitial velocity of 2.25 m/s. This corresponds to the range of traditional low-intensity magnetic separators, where the goal is to separate ferromagnetic materials [40]. Since the primary goal here is to recover the casing, a simple low-intensity magnetic separation would be sufficient.

Regarding interstitial velocity, a parameter specific to high-intensity magnetic separators, information is limited. For example, Yu et al. [46] reported using an interstitial velocity of 0.05 m/s in a simulation for high-intensity magnetic separation of LFP recovery. In contrast, the optimal model here shows the opposite: a higher interstitial velocity to prevent the capture of NMC particles. This is because materials like casing, which are much more magnetic than the paramagnetic NMC, do not need a slow velocity for effective separation. The model thus suggests the possibility of using high-intensity, high-gradient magnetic separation for recovering NMC, an option that may be worth exploring in new designs.

3.5.3. *Milling and screen*

The optimal conditions identified for the second milling unit were SGE of 5.61 kWh t^{-1} and a slope of 2.1 suggesting a smaller particle size with a narrow distribution. The P_{80} was reduced from 165 μm to 57 μm, which is ideal, as particle sizes below 250 μm are optimal for the flotation of anode and cathode materials [20]. However, it is important to note that excessive grinding can have a negative effect, especially in froth flotation, where the production of ultra fine particles can lead to entrainment [26]. Moderate grinding is more beneficial, as it helps separate the binder from the cathode, reducing the hydrophobicity of cathode materials [35]. The optimal values obtained for milling and screening parameters offer an interesting approach. Cathode and anode active materials, before being coated onto their respective current collectors, have particle sizes of around 20 μm. Therefore, when dealing with layers of cathode and anode that are reduced to such small particle sizes, the liberation increases. However, the screener, with an aperture size of 2500 μm and an alpha value of 14, suggests that no material should report to the overflow. A sharpness value of 14 indicates a highly efficient separation process, with minimal overlap between particles classified as oversize or undersized. According to the model, 5 % of each material is recovered in the overflow (>2500 μm), but this value rather reflects a restriction of maximum efficiency set at 95 %. The values identified as optimal make sense since they result in an almost perfect separation, although admittedly, this may be unrealistic in practice.

3.5.4. *Flotation circuit*

The work buy Vanderbruggen et al. [35], used model BM (pristine cathode and Gr) showing that Gr has fast flotation kinetics (>0.9 min^{-1}), with near-perfect recoveries of up to 100 % following first-order kinetics. In contrast, NMC recoveries in the concentrate are lower, ranging from just 3 % to 9 %. However, the situation changes when the materials are not fully liberated. The heterogeneity of the BM, combined with the binder in the cathode, presents a significant challenge for froth flotation. Both Ruismaki et al. and Vanderbruggen et al. [27,35] have

demonstrated that the presence of materials like Al, Cu, plastics, and binder in the cathode affects the flotation kinetics of both Gr and NMC. The work by Ruismaki et al. [27] also outlined a separation process aimed at creating two distinct streams: one for producing Ni-slag, where the cathode is reduced to nickel and Gr is used as a reduction agent, and another stream primarily containing Cu and Al. Similarly, the promise of the flotation cell in P3 follows this approach but focuses on obtaining one stream rich in Cu and Al, and another containing Gr and NMC, which would undergo further froth flotation. In this case, pre-attrition conditioning with kerosene as the collector and MIBC as the frother is used.

Gr's flotation rates, between 0.4 and 0.6 min^{-1}, are faster than those of cathode materials (NMC, LCO, and NCA), which range from 0.2 to 0.5 min^{-1}. The infinite recovery (R_∞) of Gr is also much higher, typically 85–100 %, compared to just 3–27 % for cathode materials [35,37]. For materials like Al and Cu, flotation rates are as low as 0.065 min^{-1}, with maximum recoveries of only 11 % in the concentrate [27]. This shows that Gr and NMC can be separated relatively quickly with good recoveries within short flotation times (5–10 min). In theory, given the slow kinetics and low infinite recoveries of cathode materials, it would be beneficial to float Gr as quickly as possible, allowing the cathode to go to the tailings and avoid contamination in the concentrate. However, the optimal values indicate flotation residence times of over 30 min for both cells. This suggests that to maximize both grade and recovery, the residence time should be as long as possible. With fast kinetics (0.66 min^{-1}) for Gr and NMC in the first flotation cell, and the slow recovery rate of NMC (maximum 3 % R_∞) after pre-attrition, extending the recovery time ensures better outcomes, even though the infinite recovery (R_∞) is limited. This approach seems counterintuitive to real-world operations, where shorter flotation times are typically preferred. Nevertheless, the products were obtained with a maximum Gr grade of 90.91 % and a recovery of 65 %, while NMC achieved a grade of 96.04 % and a recovery of 65 %. These optimal values are technically sound, even if they differ from practical expectations.

4. Conclusions

This study presents a first methodology to apply a data-driven approach in the design of LIB recycling processes. By using HSC-Sim® process simulation software, the research explored thousands of scenarios in a short time to identify under which process parameters it is possible to obtain NMC and Gr with acceptable values of grade and recovery for direct remanufacturing. Through a series of design iterations, a process was reached that provides superior levels of consistency and efficiency compared with the initial design concept. To achieve this, we developed a workflow to perform the simulations on a high-performance computing (HPC) system, enabling high-throughput data generation and efficient parallel execution. The vast data generated also allowed the use of a MOO to identify optimal operating conditions, highlighting the potential of big data analytics in enhancing recycling technologies.

Among the key benefits of this data-driven approach is its ability to handle complex systems by leveraging extensive datasets and advanced data analytics. This methodology not only provides objective guidelines on the robustness and adaptability of the recycling process but also supports informed decision-making and process optimization. Admittedly, this approach also has some downsides, the most evident being that the accuracy of process simulation heavily depends on the models used. Indeed, building detailed models can be expensive and requires an in-depth analysis of reliable data. Additionally, simulations might overlook unforeseen operational challenges or real-world variations, posing the risk of sub-optimal designs. Despite these challenges, the concept of integration of big data analytics into process design might develop into a valuable tool for the evaluation and design of complex transformative systems, such as those required for the efficient recycling of high technological products.

As demonstrated hereby, the integration of data-driven methodologies into process design can help address the critical needs for resource conservation and environmental protection. This study not only introduces a methodology for LIB recycling but also provides a practical example of how systematic computational screening can support industrial-scale process design. The insights gained from this work could be further utilized in developing decision-support tools for recycling technologies. Future research should focus on refining the model process and exploring new parameters to further improve recovery rates and process efficiency.

CRediT authorship contribution statement

Nima Emami: Writing – original draft, Methodology, Investigation, Data curation. **Luis Arturo Gomez-Moreno:** Writing – original draft, Methodology, Investigation, Formal analysis. **Anna Klemettinen:** Writing – review & editing, Supervision. **Rodrigo Serna-Guerrero:** Writing – review & editing, Supervision, Funding acquisition, Conceptualization. **Milica Todorović:** Writing – review & editing, Supervision, Funding acquisition, Formal analysis.

Declaration of competing interest

The authors declare that they have no known competing financial interests or personal relationships that could have appeared to influence the work reported in this paper.

Acknowledgments

This work was supported by the Research Council of Finland under the project Optimising the Circular Economy of Batteries with Artificial Intelligence Aided Designs (SmartCycling), Grant no: 347232.

Appendix A. Supplementary material

Supplementary data to this article can be found online at https://doi.org/10.1016/j.cej.2025.161128.

Data availability

The dataset supporting this study is publicly available on the Zenodo repository and can be accessed via the following DOI: https://doi.org/10.5281/zenodo.15041452.

References

[1] A. Agrawal, A. Choudhary, Perspective: materials informatics and big data: realization of the "fourth paradigm" of science in materials science, APL Mater. 4 (5) (2016).
[2] A.-R. Ali, N. Bartie, J. Husmann, F. Cerdas, D. Schröder, C. Herrmann, Simulation-based life cycle assessment of secondary materials from recycling of lithium-ion batteries, Resour. Conserv. Recycl. 202 (Mar. 2024) 107384.
[3] R. Antti and P. Kobylin. HSC Chemistry Package, 2022.
[4] D. Arellano-Sanchez, M. Rinne, B.P. Wilson, M. Lundström, Life cycle assessment of lto-rich anode waste from lithium-ion battery with a hazardous waste management approach, Resour. Conserv. Recycl. 215 (2025) 108058.
[5] Z.J. Baum, R.E. Bird, X. Yu, J. Ma, Lithium-ion battery recyclingoverview of techniques and trends, ACS Energy Lett., 7 (2) (2022) 712–719.
[6] D. A. C. Beck, J. M. Carothers, V. R. Subramanian, and J. Pfaendtner. Data science: Accelerating innovation and discovery in chemical engineering. *AIChE Journal*, 62 (5):1402–1416, 2016._eprint: https://onlinelibrary.wiley.com/doi/pdf/10.1002/aic.15192.
[7] E. Commission and D.-G. for Communication. *Circular economy action plan – For a cleaner and more competitive Europe*. Publications Office of the European Union, 2020.
[8] Q. Dehaine, L. T. Tijsseling, H. J. Glass, T. Törmänen, and A. R. Butcher. Geometallurgy of cobalt ores: A review. 160:106656.
[9] R. Denysiuk and A. Gaspar-Cunha. Weighted stress function method for multiobjective evolutionary algorithm based on decomposition. In *Evolutionary Multi-Criterion Optimization: 9th International Conference, EMO 2017, Münster, Germany, March 19–22, 2017, Proceedings 9*, pages 176–190. Springer, 2017.

[10] G. Ding, F. Liu, X. Fan, X. Gao, G. Cao, J. Ban, Z. Li, J. Hu, Research on green recycling of lithium-ion batteries cathode waste powder, Chem. Eng. J. 493 (2024) 152837.

[11] N. Emami, L. A. Gomez-Moreno, A. Klemettinen, R. Serna-Guerrero, and M. Todorović. A novel approach for data-driven design of battery recycling processes. In *Proceedings of the XXXI International Mineral Processing Congress*. Society for Mining, Metallurgy Exploration, 2024.

[12] N. Ganguli and K. S. Krishnan. Magnetic and other properties of the free electrons in graphite. *Proceedings of the Royal Society of London. Series A. Mathematical and Physical Sciences*, 177(969):168–182, Jan. 1997. Publisher: Royal Society.

[13] V. Haas, A. Waas, A. Jentzsch, J. Puetz, N. Niese, T. Lux, M. Kim, and E. Li. EV battery recycling capacity by country 2023.

[14] Z. Hu, J. Liu, T. Gan, D. Lu, Y. Wang, X. Zheng, High-intensity magnetic separation for recovery of LiFePO4 and graphite from spent lithium-ion batteries, Sep. Purif. Technol. 297 (Sept. 2022) 121486.

[15] D. Klenam, T. Asumadu, M. Vandadi, N. Rahbar, F. McBagonluri, and W. Soboyejo. Data science and material informatics in physical metallurgy and material science: An overview of milestones and limitations. *Results in Materials*, page 100455, 2023.

[16] Y. Liu, B. Ma, Y. Lü, C. Wang, and Y. Chen. A review of lithium extraction from natural resources. 30(2):209. Publisher: Nature Publishing Group.

[17] B. Makuza, Q. Tian, X. Guo, K. Chattopadhyay, and D. Yu. Pyrometallurgical options for recycling spent lithium-ion batteries: A comprehensive review. 491: 229622.

[18] McKinsey and Company. Lithium-ion battery demand forecast for 2030 | McKinsey.

[19] P. Meshram, Abhilash, and B. D. Pandey. Advanced review on extraction of nickel from primary and secondary sources. 40(3):157–193. Publisher: Taylor & Francis_ eprint: https://doi.org/10.1080/08827508.2018.1514300.

[20] S. Nazari, A.B. Vakylabad, K. Asgari, J. Li, H. Khoshdast, Y. He, A. Hassanzadeh, Bubbles to batteries: a review of froth flotation for sustainably recycling spent lithium-ion batteries, J. Storage Mater. 84 (Apr. 2024) 110702.

[21] M. Pigłowska, B. Kurc, P. Fuć, N. Szymlet, Novel recycling technologies and safety aspects of lithium ion batteries for electric vehicles, J. Mater. Cycles Waste Manage. 26 (5) (Sept. 2024) 2656–2669.

[22] H. Pinegar, Y.R. Smith, End-of-life lithium-ion battery component mechanical liberation and separation, JOM 71 (12) (Dec. 2019) 4447–4456.

[23] E.N. Pistikopoulos, Y. Tian, Advanced modeling and optimization strategies for process synthesis, Annu. Rev. Chem. Biomol. Eng. 15 (2024) 81–103.

[24] F. Punt, S. Doose, A.-C. Böttcher, S. Breitung-Faes, and Kwade, and Arno. Modeling and Flow Sheet Simulation of Selected Mechanical Recycling Processes for Li-Ion Batteries. *Chemie Ingenieur Technik*, 95(1–2):59–67, 2023._eprint: https://onlinelibrary.wiley.com/doi/pdf/10.1002/cite.202200156.

[25] M. Rinne, H. Elomaa, A. Porvali, M. Lundström, Simulation-based life cycle assessment for hydrometallurgical recycling of mixed LIB and NiMH waste, Resour. Conserv. Recycl. 170 (July 2021) 105586.

[26] T. Rinne, N. Araya-Gómez, and R. Serna-Guerrero. A Study on the Effect of Particle Size on Li-Ion Battery Recycling via Flotation and Perspectives on Selective Flocculation. *Batteries*, 9(2):68, Feb. 2023. Number: 2 Publisher: Multidisciplinary Digital Publishing Institute.

[27] R. Ruismäki, T. Rinne, A. Dańczak, P. Taskinen, R. Serna-Guerrero, and A. Jokilaakso. Integrating Flotation and Pyrometallurgy for Recovering Graphite and Valuable Metals from Battery Scrap. *Metals*, 10(5):680, May 2020. Number: 5 Publisher: Multidisciplinary Digital Publishing Institute.

[28] H. Sahivirta, B.P. Wilson, M. Lundström, R. Serna-Guerrero, A study on recovery strategies of graphite from mixed lithium-ion battery chemistries using froth flotation, Waste Manag. 180 (2024) 96–105.

[29] R. Saneie, H. Abdollahi, S. Ghassa, D. Azizi, and S. Chehreh Chelgani. Recovery of copper and aluminum from spent lithium-ion batteries by froth flotation: A sustainable approach. *Journal of Sustainable Metallurgy*, 8(1):386–397, Feb 2022.

[30] G. Schubert, S. Bernotat, Comminution of non-brittle materials, Int. J. Miner. Process. 74 (Dec. 2004) S19–S30.

[31] R. K. Sinnott. CHAPTER 1 - Introduction to Design. In R. K. Sinnott, editor, *Coulson and Richardson's Chemical Engineering (Second Edition)*, Chemical Engineering Technical Series, pages 1–31. Pergamon, Amsterdam, Jan. 1993.

[32] G. Tas, A. Klemettinen, and R. Serna-Guerrero. Circular And Sustainable: Evaluating Lithium-Ion Battery Recycling using a Combined Statistical Entropy and Life Cycle Assessment Methodology. *ChemSusChem*, n/a(n/a):e202400376._eprint: https://onlinelibrary.wiley.com/doi/pdf/10.1002/cssc.202400376.

[33] D. A. Van Veldhuizen, G. B. Lamont, et al. Evolutionary computation and convergence to a pareto front. In *Late breaking papers at the genetic programming 1998 conference*, pages 221–228. Citeseer, 1998.

[34] A. Vanderbruggen, N. Hayagan, K. Bachmann, A. Ferreira, D. Werner, D. Horn, U. Peuker, R. Serna-Guerrero, and M. Rudolph. Lithium-Ion Battery Recycling Influence of Recycling Processes on Component Liberation and Flotation Separation Efficiency. *ACS ES&T Engineering*, 2(11):2130–2141, Nov. 2022. Publisher: American Chemical Society.

[35] A. Vanderbruggen, A. Salces, A. Ferreira, M. Rudolph, and R. Serna-Guerrero. Improving Separation Efficiency in End-of-Life Lithium-Ion Batteries Flotation Using Attrition Pre-Treatment. *Minerals*, 12(1):72, Jan. 2022. Number: 1 Publisher: Multidisciplinary Digital Publishing Institute.

[36] O. Velázquez-Martínez, J. Valio, A. Santasalo-Aarnio, M. Reuter, and R. Serna-Guerrero. A Critical Review of Lithium-Ion Battery Recycling Processes from a Circular Economy Perspective. *Batteries*, 5(4):68, Dec. 2019. Number: 4 Publisher: Multidisciplinary Digital Publishing Institute.

[37] L. Verdugo, L. Zhang, K. Saito, W. Bruckard, J. Menacho, A. Hoadley, Flotation behavior of the most common electrode materials in lithium ion batteries, Sep. Purif. Technol. 301 (Nov. 2022) 121885.

[38] M. Vierunketo, A. Klemettinen, M. A. Reuter, A. Santasalo-Aarnio, and R. Serna-Guerrero. A multi-dimensional indicator for material and energy circularity: Proof-of-concept of exentropy in Li-ion battery recycling. *iScience*, 26(11):108237, Nov. 2023.

[39] Z. Wang, Z. Sun, H. Yin, X. Liu, J. Wang, H. Zhao, C.H. Pang, T. Wu, S. Li, Z. Yin, et al., Data-driven materials innovation and applications, Adv. Mater. 34 (36) (2022) 2104113.

[40] B. A. Wills and J. A. Finch. Chapter 13 - Magnetic and Electrical Separation. In B. A. Wills and J. A. Finch, editors, *Wills' Mineral Processing Technology (Eighth Edition)*, pages 381–407. Butterworth-Heinemann, Boston, Jan. 2016.

[41] E. Worrell and M. A. Reuter. Front Matter. In E. Worrell and M. A. Reuter, editors, *Handbook of Recycling*, page iii. Elsevier, Boston, Jan. 2014.

[42] L. Wuschke, H.-G. Jäckel, T. Leißner, U.A. Peuker, Crushing of large Li-ion battery cells, Waste Manage. 85 (Feb. 2019) 317–326.

[43] J. Xu, H.R. Thomas, R.W. Francis, K.R. Lum, J. Wang, B. Liang, A review of processes and technologies for the recycling of lithium-ion secondary batteries, J. Power Sources 177 (2) (Mar. 2008) 512–527.

[44] Y. Xu, X. Liu, X. Cao, C. Huang, E. Liu, S. Qian, X. Liu, Y. Wu, F. Dong, C.-W. Qiu, J. Qiu, K. Hua, W. Su, J. Wu, H. Xu, Y. Han, C. Fu, Z. Yin, M. Liu, R. Roepman, S. Dietmann, M. Virta, F. Kengara, Z. Zhang, L. Zhang, T. Zhao, J. Dai, J. Yang, L. Lan, M. Luo, Z. Liu, T. An, B. Zhang, X. He, S. Cong, X. Liu, W. Zhang, J.P. Lewis, J.M. Tiedje, Q. Wang, Z. An, F. Wang, L. Zhang, T. Huang, C. Lu, Z. Cai, F. Wang, J. Zhang, Artificial intelligence: a powerful paradigm for scientific research, The Innovation 2 (4) (Nov. 2021) 100179.

[45] Y. Yao, M. Zhu, Z. Zhao, B. Tong, Y. Fan, and Z. Hua. Hydrometallurgical processes for recycling spent lithium-ion batteries: A critical review. 6(11):13611–13627. Publisher: American Chemical Society.

[46] D. Yu, Z. Huang, B. Makuza, X. Guo, and Q. Tian. Pretreatment options for the recycling of spent lithium-ion batteries: A comprehensive review. 173:107218.

[47] A. Zanoletti, E. Carena, C. Ferrara, and E. Bontempi. A Review of Lithium-Ion Battery Recycling: Technologies, Sustainability, and Open Issues. *Batteries*, 10(1): 38, Jan. 2024. Number: 1 Publisher: Multidisciplinary Digital Publishing Institute.

[48] Y. Zhao, X. Yuan, L. Jiang, J. Wen, H. Wang, R. Guan, J. Zhang, G. Zeng, Regeneration and reutilization of cathode materials from spent lithium-ion batteries, Chem. Eng. J. 383 (2020) 123089.

[49] A.A. Zorpas, The hidden concept and the beauty of multiple "r" in the framework of waste strategies development reflecting to circular economy principles, Sci. Total Environ. 952 (2024) 175508.